Structural and Electrical Characterization of Solution-Processed Electrodes for Piezoelectric Polymer Film Sensors

Structural and Electrical Characterization of Solution-Processed Electrodes for Piezoelectric Polymer Film Sensors

Satu Rajala, Marja Mettänen and Sampo Tuukkanen

***Abstract*—Solution-processable graphene and carbon nanotube (CNT) based electrode materials were used here to provide electrodes on flexible piezoelectric polyvinylidenefluoride (PVDF) sensors. Piezoelectric sensitivity measurements, image based analysis, adhesion tests and sheet resistance measurements, were applied to these printable sensors to rigorously analyze their performance and structure. The printable sensors showed electrical performance similar to metallized sensors, whereas the adhesion of the solution-processed materials to the substrate is not as high as that of the evaporated metal films. This also affects the measured sensor sensitivity values. The measurements based on optical images were found to be a promising method to capture detailed information about the electrode surface structure.**

***Index Terms*— Printed electrodes, image analysis, measurement, piezoelectric films, piezoelectric transducers.**

I. Introduction

CARBON based nanomaterials, such as carbon nanotubes (CNT) [1, 2] and graphene [1, 3, 4] are promising materials for future electronics, photonics and materials sciences. For instance, these materials can be used as stretchable [5] and transparent [6] electrodes for sensor applications. At present, carbon based nanomaterials can be solution processed, which enables the use of printing techniques that provide a way for low-cost and high-throughput mass manufacturing of electrodes or electronic devices.

Printing techniques have been proposed as potential alternative manufacturing methods for electronics, which has opened a new field of research and development called printed electronics [7]. However, it is not known whether the solution-processed materials and structures can reach as high performance as those obtained with conventional manufacturing techniques, such as lithography and silicon microfabrication techniques. In the context of printed sensors studied in this work, profound evaluation of solution-processed electrode materials is important to find out the potential of printable materials in comparison to conventional sensor electrode materials, usually evaporated or sputtered metals.

S. Rajala, M. Mettänen and S. Tuukkanen are with the Department of Automation Science and Engineering, Tampere University of Technology, P.O. Box 692, Tampere, FI-33101 Finland (e-mail: satu.rajala@tut.fi, marja.mettanen@tut.fi, sampo.tuukkanen@tut.fi).

Polyvinylidenefluoride (PVDF) is a piezoelectric viscoelastic material that generates a charge when it is mechanically deformed [8]. Thin and flexible sensors made of PVDF (and its copolymer (PVDF-TrFE)) have a wide range of applications in the field of mechanical (e.g. pressure, acceleration, vibration and tactile sensors etc.), acoustics and infra-red-radiation sensors [9]. Other possible application areas include energy conversion [10] and medical measurements, e.g., measurement of vital signals such as heart rate and respiration [11, 12] or plantar pressure distribution measurements [13, 14].

Here the electrodes are solution-processed on a 28 µm thick PVDF material. Two graphene based ink-jet and screen formulated printable inks and one CNT based ink were chosen to be used as electrode materials. The electrodes are characterized here with sheet resistance measurements and adhesion tests. The sensor sensitivities in longitudinal and transverse directions are measured to evaluate the operation in sensor applications. Finally, the surface and the microstructure of the electrodes are evaluated with image based measurement methods.

II. Materials and Methods

A. Piezoelectric polymer PVDF

PVDF is a piezoelectric semicrystalline polymer having a solid and homogenous structure [15]; the morphology consists of crystallites dispersed within amorphous regions [16]. Piezoelectricity is a cross-coupling effect between the elastic variables (stress X and strain S) and the dielectric variables (electric displacement D and electric field E) [16]. The combinations of these variables defines the piezoelectric coefficient d, see Eq. 1 [16, 17, 18]. The first definition refers to the direct piezoelectric effect and the second one to the converse effect [17].

$$d = \left(\frac{\partial D}{\partial X}\right)_E = \left(\frac{\partial S}{\partial E}\right)_X \quad (1)$$

The piezoelectric coefficient d_{mn} is related to the electric field produced by a mechanical stress; m = 1, 2, 3 refers to the electrical axis and n = 1, 2, …, 6 refers to the mechanical axis

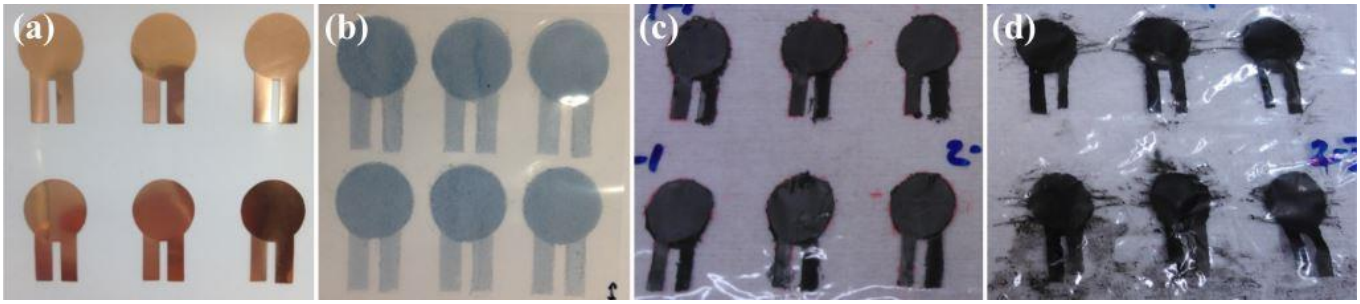

Fig. 1. The PVDF sensors with a) copper electrodes (reference) and solution-processable electrode materials (Phene-ink (b), Vor-ink (c) and CNT-ink (d)).

[8, 18]. The d_{mn} is a third-rank tensor conventionally expressed in terms of 3 × 6 matrix, however, crystal symmetry reduces the number of independent piezoelectric coefficients [19]. For the orthotropic PVDF material the matrix can be written as [17]

$$d_{mn} = \begin{pmatrix} 0 & 0 & 0 & 0 & d_{15} & 0 \\ 0 & 0 & 0 & d_{24} & 0 & 0 \\ d_{31} & d_{32} & d_{33} & 0 & 0 & 0 \end{pmatrix} \qquad (2)$$

An unmetallized, 28 µm thick PVDF film manufactured by Measurement Specialties Inc. (Hampton, USA) was used in this study.

B. Inks

Two types of graphene based commercial printable inks and one CNT based ink were used in this work. The first graphene based ink, PHENE+ I3015 (referred as Phene-ink later) was purchased from Innophene Co., Ltd (Bangkok, Thailand). The Phene-ink is an aqueous dispersion containing 1-5 wt-% poly(3,4-ethylenedioxythiophene)-poly(styrenesulfonate) (PEDOT:PSS), 1-5 wt-% graphene, 5–10 wt-% diethylene glycol and 1–5 wt-% ethanol. The ink has a solid content of 0.6 wt-% and viscosity of 7.2 mPas. It has been previously observed by TEM (transmission electron microscopy) imaging that the graphene flakes in Phene-ink are homogeneously dispersed in the polymer matrix [5]. Since the ink is made for ink-jet printing, it has low solid content and low viscosity. The low graphene and conducting polymer (PEDOT:PSS) content makes the Phene-ink film quite transparent.

The second graphene based ink, Vor-ink X103 (referred as Vor-ink later), was purchased from Vorbeck Materials Corp. (Jessup, USA). The ink has a solid content of 15-17 wt-%. The Vor-ink contains 55 wt-% hexanol, 25 wt-% amide, 15 wt-% graphite pigment, 5 wt-% polymer/solids, 2 wt-% acid catalyst and 1 wt-% 4,4-dihydroxybiphenyl. Vor-ink is highly concentrated and highly viscous as it is made especially for screen printing.

The CNT based ink (referred as CNT-ink later) is a CNT/xylan nanocomposite ink manufactured by a collaborator (Morphona Ltd., Jyväskylä, Finland). The preparation of CNT dispersions is a challenging task in general, however, xylan has been found to be a very effective dispersing agent for CNTs and it enables the fabrication of highly concentrated and stable CNT dispersions. The ink preparation in details as well as the electron microscopy characterization of the ink is described in [20]. Briefly, 3.5 wt-% of multi-walled carbon nanotubes (MWNT) were dispersed by ultrasonic mixing in aqueous solution with 1.75 wt-% xylan. The MWNTs with average diameter of 9.5 nm and carbon purity of 90 % (NC7000 series) were purchased from Nanocyl (Auvelais, Belgium).

C. Electrode fabrication

The suitable coating method for each ink was selected based on the ink viscosity. Similar electrodes were subsequently patterned on both sides of the PVDF substrate and baked after each patterning step. For all inks, a mechanical mask made of a 125 µm thick polyethylene terephthalate (PET) film was used to produce electrode patterns on a PVDF substrate. The electrodes on the two sides of the PVDF film were aligned on top of each other by eye.

Spray coating with a manual airbrush was used to deposit the Phene-ink electrodes. The current study utilizes the same Phene-ink sensor samples as used in a previous study; the electrode fabrication is described in detail in [21].

Bar coating with a manual wire bar (12 µm groove structure) was used to deposit the Vor-ink and the CNT-ink electrodes. A temporary bonding adhesive (Zig 2-Way Glue) was used to attach the mechanical mask on PVDF and to prevent the spreading of ink beneath the mask. The Vor-ink and the CNT-ink samples were baked 10 min at 60 °C in a convection oven after each bar-coating step.

Copper electrodes for the reference sensors were produced using an e-beam evaporator (Leybold Heraeus, model L 560E, Germany). The 100 nm thick electrodes were evaporated on both sides of the PVDF substrate, using a mechanical mask to produce the sensor electrode pattern.

The sensors with copper electrodes and solution-processed electrodes are shown in Fig. 1. Four sensors of each type are used; a complete row of sensors (marked as R1-1, R1-2 and R1-3) and the first sensor from the second row (marked as R2-1). Fig. 2 shows the sensor size in details.

D. Scanning electron microscopy

The microstructure of the solution-processed electrodes was studied using scanning electron microscopy (SEM). Field-emission SEM (JEOL JSM-6335F) with 5 kV acceleration voltage was used for the imaging. Before the imaging the sensors were cut mechanically with a microtome. The average

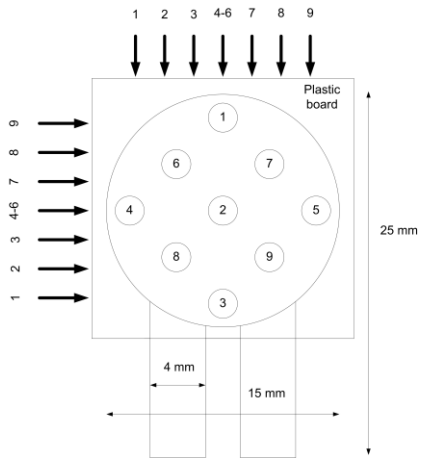

Fig. 2. The sensor size. The excitation points for the sensor sensitivity measurements in longitudinal (n = 3) and transverse (n = 1 and n = 2) directions are numbered in the figure.

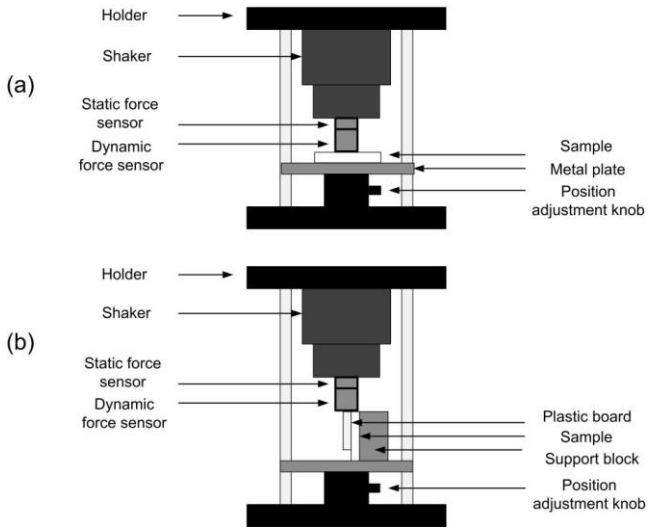

Fig. 3. The sensor sensitivity testing measurement setup for a) longitudinal direction (n = 3) and b) transverse directions (n = 1 or n = 2).

film thickness for each electrode material was obtained by taking the average of thicknesses measured from 10 separate locations from several SEM images.

E. Sheet resistance measurement and adhesion test

A multimeter (Keithley 2425) and an in-house four-point probe were used in sheet resistance measurements. Sheet resistance was measured from five different positions from each fabricated electrode. The details of the sheet resistance measurements are previously published [12, 21].

The adhesion of the deposited electrodes on the PVDF material was measured using a tape test method. Adhesion classification is done according to the ASTM standard D 3359-97 (Standard Test Methods for Measuring Adhesion by Tape Test) by applying and removing pressure sensitive tape over cuts made in the ink [22].

F. Sensor sensitivity measurements

The Brüel & Kjaer Mini-Shaker Type 4810 was used in the sensor sensitivity measurements. The shaker generates a mechanical movement, providing a dynamic excitation force for the sensor. A high sensitivity dynamic force sensor (PCB Piezotronics) was used as a reference sensor for the dynamic excitation force. A load cell (Measurement Specialties Inc.) was used as the reference sensor to measure the static force between the sample and the shaker piston. A preload, which is producing static force, is needed to keep the sample in place and to prevent the piston jumping off the surface during the measurement.

The measurement setup has been previously reported by Kärki *et al*. [13] and Rajala *et al.* [21]. Similar measurements are also done by e.g. Seminara *et al*. [23]. To measure the sensor sensitivity in longitudinal direction (n = 3), the sensor was placed horizontally on the metal plate, see Fig. 3a. A 125 µm thick PET film was used for electrical insulation. A static force of approximately 3 N was used. The sensor was excited with a dynamic sinusoidal normal force of 1.3 N (peak to peak) and frequency of 2 Hz. The tip of the dynamic force sensor was 4 mm in diameter; the area of this tip was in contact with the studied PVDF sample. The effect of frequency on piezoelectric coefficients has been previously studied by Seminara *et al*. [23] and Rajala *et al*. [21]. Based on the findings of these studies, only one frequency of 2 Hz is used in this study. The excitation was done by applying the force to 9 different positions on the sensor (visual estimation), one at a time (see Fig. 2). The same positions were excited from both sides of the sensor, resulting in a total of 18 excitations per sensor. The measured sensitivity in the longitudinal direction is closely related to piezoelectric d_{33} coefficient. The longitudinal d_{33} coefficient describes the electric polarization generated in the same direction as the stress applied [24].

In sensitivity measurements in transverse directions (n = 1 and n = 2), the sensors were attached in a vertical position. A metal support block and a plastic board were used to keep the element in this position, see Fig. 3b. Double-sided tape (3M) was used in the attachments between the plastic board and the sensor and between the sensor and the support block. The dynamic force was exerted on the plastic board to stretch the sensor in the direction of mechanical axes n = 1 or n = 2 and thus to generate a shear stress. These two directions were measured separately. Compared to the sensitivity measurements in direction n = 3, a smaller static force of approximately 1 N was adjusted. Also a smaller dynamic excitation force was used due to the smaller cross-sectional area of the sensor (0.13 N (peak to peak)). The excitation was done by applying the force to 9 different positions of the plastic board (see Fig. 2). With this measurement setup, the sensor sensitivities in the directions of the mechanical axes n = 1 and n = 2 are measured, not the actual d_{31} and d_{32} coefficients. The actual shear coefficients d_{15} and d_{24} are not measured here either. The sensor sensitivities measured here are needed for instance in plantar shear stress measurements [13, 14].

The charge developed by the sensor was measured with a custom-made combination of a charge amplifier and a 16-bit

AD-converter. The connection to the AD-converter from the sensor was provided via coaxial wires and crimp connectors (Nicomatic Crimpflex). The measured data was processed to solve the sensitivity of the sensor to the force. The sensitivity was obtained by dividing the charge generated by the sensor with the force obtained with the dynamic force sensor. The unit of sensitivity is thus pC/N.

G. Measurements based on optical images

All the 12 sensors with solution-processed electrodes were photographed from both sides using a photometric stereo setup, to capture detailed information about their surface structure. Photometric stereo provides a fast non-contact method for estimating the surface orientation at each point (pixel) [25], which gives an indication of surface roughness. The setup consists of a camera that is situated right on top of the sample, and light sources in slant angles; see Fig. 4. In our setup, 12 images are taken of the sample with different illumination directions while the sample lies still on a white table. The inference of the surface orientation (i.e., gradients) from these intensity images relies on the assumption that the intensity in a point depends directly on the gradient values at that point, given the imaging geometry and additional assumptions about the surface reflection model. Photometric stereo is widely used in computer graphics for surface analysis and reconstruction (e.g. [26]), and applications in small-scale surface topography measurement can be found, e.g., in paper industry [27] and dermatology [28].

The photographs were captured using a digital systems camera (Canon EOS 550D) and a 105 mm macro lens from Sigma. The photosensitive silicon sensor of the camera has 18 megapixels in an area of 22.3 mm by 14.9 mm. Thus, the PVDF sensors with diameter of 15 mm barely fitted to the field of view of the camera with 1:1 magnification, and this resulted in the pixel size of 4.3 µm by 4.3 µm.

The illumination was implemented with 12 green LEDs (light-emitting diodes), grouped into three groups to enable illumination from three different heights, namely angles $\sigma = 75°$, $\sigma = 60°$ and $\sigma = 45°$ in Fig. 4. The larger the polar angle σ, the more the illumination emphasizes small spots and shallow indentations on the surface of the object. In each LED group, the LEDs were positioned at azimuth angles (τ) 90° apart from each other.

The surface topography of the sensors with Vor-ink and CNT-ink electrodes was investigated through the surface gradients in x and y directions, where x direction refers to the direction of the connectors. The standard deviation of the gradient field at various wavelengths was computed to give an indication of the surface roughness at selected size scales [29]. For the Phene-ink coated sensors, local mean and standard deviation values were computed from the photographs as such. For each image (x or y gradient, or photograph), local mean and standard deviation were computed from 9 positions according to Fig. 2, corresponding to the positions of the sensor sensitivity measurements (direction $n = 3$).

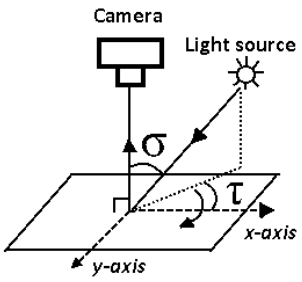

Fig. 4. Photometric stereo imaging principle. The camera was situated at polar angle $\sigma = 0°$ and the light sources were at $\sigma = 75°$, $\sigma = 60°$ and $\sigma = 45°$. For each value of σ, the four light sources (of which one is shown) had azimuth angles (τ) 90° apart from each other.

III. RESULTS

A. SEM analysis

Examples of the SEM images are shown in Fig. 5. The solution-processed electrodes are visible in the SEM images on both sides of the PVDF film. The images also show that the electrode film thicknesses vary from place to place and side to side. This is related to the solution-processing methods which are not producing highly smooth coatings. The average electrode thicknesses for Phene-ink, Vor-ink and CNT-ink on each side were (1 ± 0.5) µm, (10 ± 3) µm and (3 ± 1) µm, respectively.

B. Sheet resistance measurement and adhesion test

Table I shows the sheet resistance measurement results for the reference electrodes and the printable electrodes. Four sensors of each type were measured. Sheet resistances were measured from all electrodes and the results are presented as

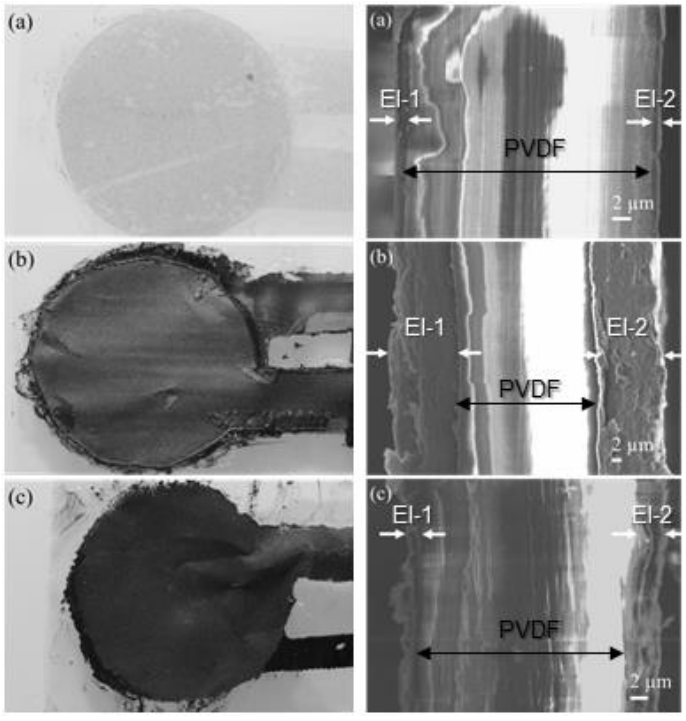

Fig. 5. Examples of the photographs and SEM images of cross-sections of PVDF sensors with a) Phene-ink (R1-1 from side 1, illumination polar angle $\sigma = 45°$), b) Vor-ink (R1-1 from side 1, illumination polar angle $\sigma = 60°$) and c) CNT-ink (R1-2 side 2, illumination polar angle $\sigma = 75°$) electrodes (El-1 = electrode 1, El-2 = electrode 2).

TABLE I
SHEET RESISTANCE MEASUREMENT AND ADHESION TEST RESULTS

Electrode material	R_S (Ω/□)	Adhesion classification
Cu ref.	1.0 ± 0.2	5B (0% detached)
Phene-ink	105.0 ± 12.0	3B (5-15% detached)
Vor-ink	46.5 ± 7.1	2B (15-35% detached)
CNT-ink	150.8 ± 18.4	1B (35-65% detached)

mean sheet resistances ± standard deviations.

The copper electrodes showed good conductivity with the average sheet resistance of 1.0 Ω/□. The Phene-ink electrodes showed a higher sheet resistance of 105.0 Ω/□ due to the thin ink layer which is needed to obtain the transparency of the electrodes. The sheet resistances of Vor-ink and CNT-ink electrodes fabricated in this work are somewhat higher than those obtained in previous studies [20, 21].

The adhesion test results are also presented in Table I. The reference copper electrodes have a very good adhesion to the PVDF substrate. Also, the Phene-ink coating has quite good adhesion to the substrate most likely due to the use of relatively thin layer (1 µm) and spray-coating technique. In order to improve the adhesion of the Vor-ink electrode material, the wire bar coating was used here instead of the doctor blade coating used in the previous study [21]. The wire bar was expected to give better adhesion than doctor blading because of the forced ink spreading by the coils of the wire bar. Unfortunately, adhesion tests showed that the adhesion was not improved from the previous study (adhesion classification 2B in the both studies). The CNT-ink coating had relatively poor adhesion, because the ink was not optimized for these type of applications and surfaces.

C. Sensor sensitivity

Table II shows the sensitivity measurement results for each sensor type. In longitudinal direction (n = 3), the results are shown as mean sensitivity ± standard deviation of 18 excitations per sensor. The sensitivity of the reference copper sensors is close to the theoretical sensitivity of the PVDF material (d_{33} = -33 pC/N [8]). This is mainly due to the high adhesion and high electrical conductivity of the metal electrodes. The sensitivity of the Vor-ink sensors appears to be very close to that of the reference copper sensors. This can be due to the Vor-ink electrode sheet resistance being 2-4 times lower than that of the Phene-ink and the CNT-ink electrodes. The sensors with bar coated Vor-ink electrodes also showed higher sensitivity value than previously when blade coated electrodes from the same material were used ((30.2 ± 1.6) pC/N versus (21.4 ± 1.3) pC/N), even though the electrode adhesion did not change [21]. This can be explained by smoother films and smaller thickness variations in the case of bar coating, which increases the coupling between the actual sensing material (PVDF) and the shaker's piston. Instead, the sensors with the CNT-ink electrodes showed sensitivities higher than the theoretical sensitivity of the PVDF material used. The CNT-ink sensors typically featured wrinkles (discussed more thoroughly in Section IIID). These wrinkles may cause force components related to both normal (n = 3) and transverse directions (n = 1 and n = 2), thus increasing the charge developed by the sensor and further, increasing the sensitivity of the sensor. This, however, cannot be proved based on these measurements. The sensors with the Phene-ink electrodes showed the lowest sensitivity value. This is expected to results from high sheet resistance of the Phene-ink electrodes.

TABLE II
SENSITIVITY MEASUREMENT RESULTS. THE UNITS ARE PC/N.

Electrode	n = 3 Side 1	n = 3 Side 2	n = 1	n = 2
Cu ref. R1-1	30.4 ± 1.1	32.2 ± 0.5	260.2 ± 4.4	32.2 ± 5.1
Cu ref. R1-2	31.4 ± 1.1	30.3 ± 1.3	261.9 ± 7.0	34.4 ± 4.7
Cu ref. R1-3	30.6 ± 0.8	31.5 ± 0.5	270.1 ± 7.1	33.1 ± 3.5
Cu ref. R2-1	32.6 ± 1.3	29.6 ± 1.3	264.6 ± 6.5	33.3 ± 3.8
Phene-ink R1-1	26.2 ± 1.2	26.7 ± 1.9	642.7 ± 52.4	24.8 ± 12.5
Phene-ink R1-2	25.5 ± 2.4	27.5 ± 2.1	696.4 ± 20.8	40.5 ± 19.7
Phene-ink R1-3	27.7 ± 2.5	25.9 ± 1.9	794.1 ± 30.9	23.5 ± 7.6
Phene-ink R2-1	26.2 ± 1.7	23.9 ± 1.5	704.1 ± 34.5	32.7 ± 10.7
Vor-ink R1-1	30.1 ± 1.7	31.2 ± 1.2	95.9 ± 6.2	19.2 ± 1.2
Vor-ink R1-2	29.2 ± 1.7	30.0 ± 1.8	212.8 ± 6.8	18.2 ± 1.6
Vor-ink R1-3	30.7 ± 1.4	29.1 ± 1.2	91.5 ± 7.8	16.0 ± 1.8
Vor-ink R2-1	31.2 ± 1.2	30.1 ± 2.0	142.3 ± 11.5	19.6 ± 2.7
CNT-ink R1-1	37.8 ± 5.9	42.3 ± 6.2	293.3 ± 16.4	30.6 ± 8.6
CNT-ink R1-2	44.5 ± 2.5	45.2 ± 4.5	137.9 ± 15.7	19.0 ± 5.8
CNT-ink R1-3	38.0 ± 7.4	39.8 ± 8.3	167.1 ± 14.7	71.5 ± 5.8
CNT-ink R2-1	44.9 ± 2.4	45.5 ± 2.2	162.7 ± 8.7	67.6 ± 5.3

Table II also shows the sensitivity measurement results for each sensor type in transverse directions (n = 1 and n = 2). The results are shown as mean sensitivity ± standard deviation of 9 excitations per sensor. The sensitivities in transverse directions measured with reference copper and Phene-ink sensors were similar inside the set of four sensors made of the same electrode material. Instead, in the case of Vor-ink and CNT-ink sensors the sensitivities showed about 50 % variation from the average sensitivity value. Poor adhesion of the electrodes is expected to lower the measured sensitivity in the case of force in directions n = 1 and n = 2, because the electrode material can partially detach from the PVDF surface during the measurement and decrease the area from which the charges are extracted from the sensor material. The high adhesion of copper and Phene-ink electrodes can explain their high sensitivity values and small sensitivity variations. However, good adhesion does not explain why Phene-ink sensor sensitivities in direction n = 1 are over two times larger than those of copper reference sensors.

The thickness of the Vor-ink electrodes (in total 2 x 10 µm) is almost equal to the thickness of the PVDF film (28 µm). In the transverse sensitivity measurements (n = 1 and n = 2) the force is applied parallel to the sensor, and thus the caused deformation is divided between the sensor film and the electrodes. This causes the decrease of actual deformation caused to the PVDF film itself, which is then decreasing the measured sensitivity in the transverse directions. The same also applies to the CNT-ink electrodes which are thicker than the Phene-ink electrodes and give also smaller sensitivity values in the transverse directions.

Based on the results obtained here, it is evident that the electrode properties, such as thickness, smoothness and conductivity affect to the way the applied force is transferred

from the shaker's piston to the actual PVDF film.

D. Measurements based on optical images

The photographs of the sensors captured the essential differences between the sensor types. Fig. 5 gives examples of the photographs. The Phene-ink sensors were partly transparent and had a very smooth surface structure. The Vor-ink and CNT-ink sensors typically featured wrinkles, and the former also had small but visible aggregates on the surface.

The aim of the image based measurements was to characterize the surface of the sensors in an objective manner, and to test whether the measurement results obtained from the images accord with the sensor sensitivity measurement results. As mentioned in Section IIG, two approaches were applied in the analysis of the optical images of the sensors; one for the Phene-ink sensors and the other for Vor-ink and CNT-ink.

The surface of the Phene-ink sensors showed no visible wrinkles or other surface height variations. Furthermore, the partly transparent Phene-ink coating on top of the transparent PVDF film severely violated the Lambertian reflection model assumption made in the surface gradient estimation, which disabled the gradient estimation. Hence, local mean and standard deviation values were computed from the photographs of the Phene-ink sensors as such (with illumination pattern due to the position of each LED compensated). Only the photographs with illumination polar angle $\sigma = 45°$ were used to minimize the effect of shadows. The intensity variations in the photographs of the Phene-ink-coated sensors express the uneven spread of the spray coating which was partly visible also to naked eye. The mean values of the photographs (in the area of the sensor) describe the intensity or thickness of the Phene-ink layer on the surface of the PVDF film. The mean and standard deviation values were compared with the sensitivity measurement results in longitudinal direction ($n = 3$).

There were 8 images of the Phene-ink sensors, resulting from 4 sensors imaged from both sides, and 9 local analysis areas per image, as shown in Fig. 2. First, the 9 mean or standard deviation values for each image were averaged, and these 8 average values were compared with the corresponding sensitivity measurements ($n = 3$) of the sensors (see Table II). No correlation was found between the sensitivities of the sensors and the mean and standard deviation of the image intensities. It was then further tested, for each sensor, whether the 9 local mean and standard deviation values correlate with the local sensitivity readings recorded from the same positions. The result was again negative. Various low-pass and high-pass filters were also applied on the images to emphasize selected size scales of the unevenness of the Phene-ink coating. The conclusion was that the local average thickness/image intensity of the Phene-ink layer, or the local variation in the thickness/image intensity, cannot directly predict the sensitivity of the sensors in this experiment.

The image analysis of the Vor-ink and CNT-ink sensors was based on the gradient fields that express the rate of change of surface height in x and y directions for each pixel. To minimize the effect of shadows that disturb the gradient estimation, the gradient image analysis of the Vor-ink and CNT-ink sensors focused on the smallest illumination angle ($\sigma = 45°$). The surface roughness of these sensors was characterized through the standard deviation of the gradient fields [29]. Although this was not calibrated to correspond to a reference roughness scale, the computed roughness parameters can be compared with each other inside this experiment. In general, the surface height variations measured by our photometric stereo correspond to reference measurements (e.g., contact profilometry) in the short wavelength scale (<1 mm in the plane of the sample) with an accuracy of approximately 10 µm. The standard deviation was computed from the 9 local areas (Fig. 2) of each high-pass or low-pass filtered gradient image. The limit wavelengths of the filters were designed to separate small aggregates of the ink layer from the larger wrinkles of the sensor.

It was found that, without filtering, the surface roughness of the Vor-ink sensors was higher than that of the CNT-ink sensors. The Vor-ink sensor images typically had x-directional streaks (i.e., aligned with the connectors) of width approximately 1 mm, and additionally waviness in the same direction with a wavelength of 10-15 millimeters. The Vor-ink electrode material had also formed small aggregates on the surface of the sensor. Low-pass filtering of the gradient images with a limit wavelength of 100 µm or longer caused the x-gradient-based roughness parameters of the Vor-ink and CNT-ink sensors to become almost equal, apparently due to the attenuation of the aggregates in the Vor-ink sensor images. Due to the streaks and waviness, the y-directional roughness parameter remained higher in Vor-ink than in CNT-ink sensors despite low-pass filtering. High-pass filtering further emphasized the roughness differences between the sensor types. The standard deviations were plotted against the sensitivity results ($n = 3$) reported in Table II, see Fig. 6. The results in Fig. 6(a) imply that in the combined data set of CNT-ink and Vor-ink sensors, the surface roughness parameter correlates negatively with the sensitivity of the sensors. This holds also within the group of CNT-ink sensors, in which the correlation coefficient is around -0.7 (p-values range from 0.04 to 0.06 depending on filtering). However, no such correlation was found within the group of Vor-ink sensors, despite the various low-pass, high-pass and band-pass filtering trials.

Closer inspection of the CNT-ink sensors showed that two of the four CNT-ink sensors had more serious wrinkles than the other two. The wrinkled ones (C1-1 and C1-3) can be seen in Fig. 6 as the four blue dots (two per sensor) with lower sensitivity readings than the other four. The average sensitivity ($n = 3$) in the wrinkled sensors was 12 % lower than that of the smoother sensors. The standard deviation of the sensitivity readings in the wrinkled sensors was more than twice as large as in the smoother CNT-ink sensors. Based on visual inspection, the local analysis areas (see Fig. 2) that were the most affected by the wrinkles were then separated from the rest of the analysis areas. This revealed that the wrinkles, when caught by the shaker's piston, tend to give rise to abnormally low or high sensitivity readings in the direction *n*

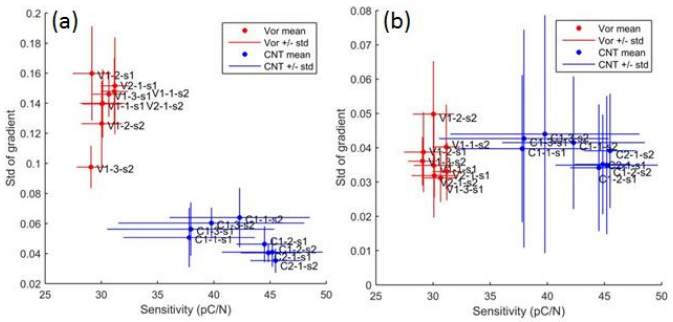

Fig. 6. Sensitivities (s1 = side 1, s2 = side 2) of the Vor-ink (V) and CNT-ink (C) sensors (n = 3) plotted against the surface roughness parameter, i.e., standard deviation (std) of the gradient. (a) Roughness parameter based on the unfiltered y-gradient images. (b) Roughness parameter based on the low-pass filtered x-gradient images; limit wavelength 100 µm.

= 3. When these wrinkled local areas were eliminated from the correlation analysis, the correlation previously detected between the surface roughness parameter and the sensitivity of the CNT-ink sensors vanished. This also explains why no such correlation was found in the Vor-ink sensor group in the first place: these sensors had very little or no wrinkles. Eliminating the most visible aggregates and the few detached flakes of Vor-ink electrode material from the image analysis of the Vor-ink sensors did not affect the negligible correlation between the surface roughness parameter and sensor sensitivity.

IV. Discussion and Conclusions

In this study, two graphene based printable inks and one CNT based ink were used as solution-processable electrode materials to manufacture piezoelectric PVDF sensors. Versatile structural and electrical characterization methods were used to analyze the performance and structure of the solution-processed electrodes. In comparison, conventional evaporated copper electrodes were used as reference sensors in sheet resistance and sensor sensitivity measurements, as well as in the adhesion tests.

The sensitivities of the sensors with solution-processed electrodes were measured in longitudinal (n = 3) and in transverse (n = 1 or n = 2) directions. Some differences in the sensitivity measurement results appeared when compared to the results obtained with the reference sensors. The sensor sensitivities are affected by the sheet resistance, adhesion and thickness of the electrodes as well as the ink and the coating method. Even if the solution-processed electrodes have a higher sheet resistance than the copper reference electrodes, it is expected to have significant effect on the sensor sensitivity only in the high frequency region [8]. The adhesion of the solution-processed electrodes on PVDF was lower than in the case of copper, which can cause fast degradation of the sensor functionality and shortens its life-time. In the case of sensitivity measurements in transverse directions, poor adhesion can decrease the sensitivity due to detachment of the electrode material. In addition, the electrode thickness may affect due to the better elasticity of thin electrodes. Finally, also the inhomogeneity of the piezoelectric polymer film may affect the measured sensitivity values.

The SEM analysis and photographs of the sensors captured the essential differences between the sensor types. Whereas the Phene-ink electrodes were thin (1 µm), smooth and partly transparent, the Vor-ink and CNT-ink electrodes were thicker (10 and 3 µm, respectively) and typically featured some wrinkles or aggregates. Small aggregates were observed in the optical analysis of the Vor-ink electrodes, which can be explained by the natural tendency of agglomeration of graphene flakes (as well as CNTs). Since the CNT-ink used here is still under development phase and is not optimized for manufacturing, it undergoes a noticeable shrinking during drying of the film. This can explain the high amount of wrinkles and curvatures in the CNT-ink sensors. CNT-ink is optimized as a stable aqueous dispersion of CNT, and thus the ink does not easily form aggregates.

The wrinkles of the CNT-ink sensors seem to increase the variance of the sensor sensitivity readings in all directions. The surface roughness of the Vor-ink electrodes was found to be higher than that of the CNT-ink sensors. However, the ink aggregates in the Vor-ink electrodes that caused this roughness difference do not have a consistent effect on sensor sensitivity, nor do the streaks and waves of the electrodes. The local variation in thickness of the Phene-ink electrodes cannot directly predict the sensitivity of the sensors. It will be interesting to further define these findings in the future with a larger set of sensors.

The optical image based analysis of the surface structure of the Phene-ink sensors turned out to be more challenging than expected due to the transparency of the ink layer. It will be interesting to run further image based measurements with a new set of sensors, and try, for instance, to replace the white background in the imaging setup with a black one. This will reduce unwanted light reflections from behind the semi-transparent sensors. Another image quality improvement would result from placing the LED lights even higher (polar angle, σ, smaller than 45°).

To conclude, the sensors with solution-processable carbon based electrode materials showed some differences when compared to sensors with evaporated copper reference electrodes. However, the sensors with solution-processed electrodes are functional and they have some advantages over the use of metallic printable inks or conventional electrode manufacturing methods. First, there is no need for high temperature sintering (as in the case of metallic printable inks), which makes the carbon based electrode materials favorable for piezoelectric PVDF due to its temperature sensitivity [12]. Second, in comparison to conventional lithography based techniques the use of solution-processable materials enables low-cost and high-throughput mass manufacturing of the discrete PVDF sensors or PVDF sensor matrices in a desired and customized shape and size using printing techniques. Also, carbon based printable materials offers routes towards greener electronics producing less waste and requiring less energy.

Acknowledgment

The authors acknowledge funding from the Academy of

Finland (Dec. No. 137669, 258124 and 138146). The authors also thank M.Sc. (Tech.) Tiina Vuorinen for preparing the Phene-ink samples and measuring sheet resistances for the reference copper and Phene-ink sensors.

REFERENCES

[1] P. Avouris, Z. Chen and V. Perebeinos, "Carbon-based electronics", *Nature Nanotechnology*, vol. 2, pp. 605-615, 2007.

[2] M.F.L. De Volder, S.H. Tawfick, R.H. Baughman and A.J. Hart, "Carbon nanotubes: Present and future commercial applications", *Science*, vol. 339, pp. 535-539, 2013.

[3] F. Bonaccorso, Z. Sun, T. Hasan and A. C. Ferrari, "Graphene photonics and optoelectronics", *Nature Photonics*, vol. 4, pp. 611–622, 2010.

[4] K.S. Novoselov, V.I. Fal'ko, L.Colombo, P.R. Gellert, M.G. Schwab and K. Kim, "A roadmap for graphene", *Nature*, vol. 490, pp. 192–200, 2012.

[5] S. Tuukkanen, M. Hoikkanen, M. Poikelispää, M. Honkanen, T. Vuorinen, M. Kakkonen, J. Vuorinen and D. Lupo, "Stretching of Solution Processed Carbon Nanotube and Graphene Nanocomposite Films on Rubber Substrates", *Synthetic Met*, vol. 19, pp. 28-35, 2014.

[6] T. Vuorinen, M. Zakrzewski, S. Rajala, D. Lupo, K. Palovuori, J. Vanhala and S. Tuukkanen, "Printable, transparent and flexible touch panels working in sunlight and moist environments", *Advanced Functional Materials*, vol. 24, pp. 6340-6347, 2014.

[7] White Paper, "OE-A Roadmap for Organic and Printed Electronics", 5th edition, Organic and Printed Electronics Association, Frankfurt, 2013.

[8] Measurement Specialties Inc., Piezo film sensors, Technical manual. Available online at: http://www.meas-spec.com (accessed 14 Feb 2015).

[9] G. Harsanyi, "Polymer films in sensor applications: a review of present uses and future possibilities", *Sensor Review*, vol. 2, pp. 98-105, 2000.

[10] S.B. Lang & S. Muensit, "Review of some lesser-known applications of piezoelectric and pyroelectric polymers", *Appl Phys A*, vol. 85, pp. 125-134, 2006.

[11] S. Rajala and J. Lekkala, "Film-type sensor materials PVDF and EMFi in measurement of cardiorespiratory signals: A review", *IEEE Sensors Journal*, vol. 12, pp. 439-446, 2012.

[12] S. Tuukkanen, T. Julin, V. Rantanen, M. Zakrzewski, P. Moilanen, K. E. Lilja and S. Rajala, "Solution-processible electrode materials for a heat-sensitive piezoelectric thin-film sensor", *Synthetic Met*, vol. 162, pp. 1987-1995, 2012.

[13] S. Kärki, J. Lekkala, H. Kuokkanen and J. Halttunen, "Development of a piezoelectric polymer film sensor for plantar normal and shear stress measurements", *Sensor Actuat A- Phys*, vol. 154, pp. 57-64, 2009.

[14] S. Rajala and J. Lekkala, "Plantar shear stress measurements – A review", *Clin Biomech*, vol. 29, pp. 475-483, 2014.

[15] G. Eberle, H. Schmidt and W. Eisenmenger, "Piezoelectric polymer electrets", *IEEE T Dielect El In*, vol. 3, pp. 624-646, 1996.

[16] J.S. Harrison and Z. Ounaies, "Polymers, Piezoelectric", Encyclopedia of Smart Materials. John Wiley & Sons, Inc., 2002.

[17] T. Furukawa, "Piezoelectricity and pyroelectricity in polymers", *IEEE T El In*, vol. 24, pp. 375-394, 1989.

[18] D.A. Berlincourt, D.R. Curran and H. Jaffe, "Piezoelectric and piezomagnetic materials and their function in transducers", in *Physical Acoustics, Principles and Methods*, Vol 1 – Part A, New York: Academic Press, 1964, pp. 169-270.

[19] J. F. Nye, *Physical Properties of Crystals*. London, U.K.: Oxford Univ. Press, 1969.

[20] S. Lehtimäki, S. Tuukkanen, J. Pörhönen, P. Moilanen, J. Virtanen, M. Honkanen and D. Lupo, "Low-cost, solution processable carbon nanotube supercapacitors and their characterization", *ApplPhys A*, vol. 117, pp. 1329-1334, 2014.

[21] S. Rajala, S. Tuukkanen and J. Halttunen, "Characteristics of piezoelectric polymer film sensors with solution-processable graphene-based electrode materials", *IEEE Sensors Journal*, vol. 15, pp. 3102-3109, 2015.

[22] Standard Test Methods for Measuring Adhesion by Tape Test, United States ASTM D3359-97, 1997.

[23] L. Seminara, M. Capurro, P. Cirillo, G. Cannata and M. Valle, "Electromechanical characterization of piezoelectric PVDF polymer films for tactile sensors in robotics applications", *Sens. Actuators A: Phys.*, vol. 169, pp. 49-58, 2011.

[24] K.S. Ramadan, D. Sameoto and S. Evoy, "A review of piezoelectric polymers as functional materials for electromechanical transducers", *Smart Mater. Struct.*, vol. 23, 26 pp., 2014.

[25] R.J. Woodham, "Photometric method for determining surface orientation from multiple images", *Opt Eng*, vol. 19, pp. 139-144, 1980.

[26] D.B. Goldman, B. Curless, A. Hertzmann and S.M. Seitz, "Shape and Spatially-Varying BRDFs from Photometric Stereo", *IEEE T Pattern Anal*, vol. 32, pp. 1060-1071, 2010.

[27] M. Mettänen, Measurement of print quality: Joint statistical analysis of paper topography and print defects, PhD Thesis, Tampere University of Technology, Tampere, Finland, 2010.

[28] A. Sohaib, A. R. Farooq, G. A. Atkinson, L. N. Smith, M. L. Smith and R. Warr, "In vivo measurement of skin microrelief using photometric stereo in the presence of interreflections", *J Opt Soc Am A Opt Image Sci Vis*, vol. 30, pp, 278-286, 2013.

[29] K. J. Stout and L. Blunt, *Three dimensional surface topography*, 2nd ed., Penton Press, London, 2000.

Satu Rajala (née Kärki) received her M.Sc. and D.Sc. (Tech.) degrees from Tampere University of Technology (TUT), Finland in 2004 and 2009, respectively. She has been working in the Department of Automation Science and Engineering, TUT since 2003. Her interest areas include sensors, sensor materials and sensor systems for physiological measurements.

Marja Mettänen received the M.Sc. degree in electrical engineering from TUT in 2003 and the D.Sc. (Tech.) degree in automation science and engineering in 2011. She has been working at TUT since 2001, first with signal processing related topics and, since December 2004, in paper and print quality research. She is currently working on the characterization of paper structure based on 2D and 3D images.

Sampo Tuukkanen received the Ph.D. degree in the Department of Physics, University of Jyväskylä, Finland, in 2006. From 2007 to 2015, he worked on areas of molecular nanomaterials and printed electronics at CEA/Saclay in France, at the Department of Electronics and Communications Engineering, TUT, and at the Department of Materials Science and Engineering, Aalto University in Finland. Since March 2015, he started as an Assistant Professor at the Department of Automation Science and Engineering, at TUT, Finland.